Synthetic Metals, 2 (1980) 57 - 84

KINETICS OF INTERCALATION AND DESORPTION IN GRAPHITE*

K. K. BARDHAN

Department of Physics,

J. C. WU and J. S. CULIK**

Department of Electrical Engineering,

S. H. ANDERSON and D. D. L. CHUNG***

Department of Metallurgy and Materials Science, Carnegie-Mellon University, Pittsburgh, PA 15213 (U.S.A.)

(Received June 7, 1980)

Summary

The kinetics of intercalation was studied by measuring the surface profile on the *c*-face and the expansion at the edge during intercalation. A phenomenological model of interface-controlled intercalation is presented and agreement between the model and various experimental results is shown. The kinetics of desorption was studied by using surface profilometry, gas detection and thermogravimetry. These experimental results suggest a phenomenological model of desorption, which considers the out-diffusion of the intercalate.

1. Kinetics of intercalation

1.1. Introduction

Graphite intercalation compounds are currently being investigated for use in such diverse applications as catalysts, batteries, and electrical conductors due to the attractive properties of intercalation compounds and the variety of intercalation compounds which form. While investigation of the structure and properties of intercalation compounds is important, it is valuable to gain an understanding of the kinetics of intercalation and desorp-

*Research sponsored by the Air Force Office of Scientific Research, Air Force Systems Command, USAF, under Grant No. AFOSR-78-3536. The United States Government is authorized to reproduce and distribute reprints for Governmental purposes notwithstanding any copyright notation hereon.

**Present Address: Solarex Corp., 1335 Piccard Dr., Rockville, MD 20850, U.S.A.

***Also in the Department of Electrical Engineering.

tion in order to provide a guide to determining the optimum conditions for producing a particular type of intercalation compound.

Intercalation is the process which results in a lamellar compound. However, a lamellar compound tends to desorb its intercalate once it is removed from the equilibrium with the intercalate vapor. Although a fraction of the intercalate is still retained in the graphite after desorption has ended, the desorbed compound has a much lower intercalate concentration than the parent lamellar compound. Therefore, understanding the kinetics of desorption is essential for practical uses of graphite intercalation compounds.

In this paper, Section 1 addresses the kinetics of intercalation and Section 2 addresses that of desorption.

The *c*-direction thickness expansion characteristic of intercalation lends itself to investigation of the kinetics of intercalation. Hooley *et al.* [1 - 3], by measuring the thickness at the sample edge and *c*-face center, demonstrated that intercalation begins at the edges of *c*-face surfaces and proceeds to the center. Saunders *et al.* [4, 5] used thickness measurements to calculate the internal constraints on expansion.

The shape deformation known as the "ashtray effect" or "window pane effect" [6] offers a simple and direct means of observing the position of the intercalated region as a function of time. For example, this effect has been used to observe the intercalation of lithium in transition metal dichalcogenides [7]. In this work the topographical profile of the *c*-face was measured during the intercalation of bromine into highly oriented pyrolytic graphite (HOPG) in order to elucidate the intercalation process. Furthermore we have measured the edge expansion of HOPG during intercalation with Br_2, ICl, and HNO_3 in a more rapid and precise manner than has hitherto been done.

1.2. Experimental techniques

1.2.1. Surface profilometry

Specimens used in profilometry were all based on HOPG (Grade ZYA) kindly provided by Union Carbide Corporation. They were cut into cylindrical discs by using a spark cutter, such that the *c*-axis was parallel to the thickness. Disc diameters vary from 4.5 to 8 mm and disc thicknesses vary typically from ~ 0.1 to 0.4 mm. Cleaving by using adhesive tape was performed to improve the smoothness of the *c*-face surface. Samples of large thickness could not be obtained due to the tendency of splitting during spark cutting. Square specimens obtained by using a wire saw were also used.

Profilometry was performed during intercalation with Br_2. Intercalation was achieved by exposing the sample to the vapor of the particular intercalate species. Various Br_2 vapor pressures were achieved by varying the temperature of the Br_2 liquid using a water bath. To obtain the variation of the surface profile during intercalation, the sample was removed from the intercalation vessel at regular intervals and its surface profile was measured at room temperature. Each measurement took, typically, about half an hour.

Occasional interruptions of the intercalation process are believed to have a negligible effect on the experimental results reported here.

The surface profile on the *c*-face was measured by the Tallysurf method using a surface profilometer (Dektak, Sloan Technical Corp.) which had a diamond stylus of radius 0.0005 in. at the tip. The stylus was allowed to move along several diameters of each disc with a pressure of 50 mg/cm^2, which is fixed by the manufacturer. The maximum range of the profilometer was 0.01 cm, which is, in most cases, less than the maximum expansion possible along the *c*-direction (55% of the sample thickness for the case of Br_2 intercalation). As a result, complete surface profiles during the entire intercalation process could not be obtained.

1.2.2. Edge expansion

The apparatus used to measure the edge thickness is similar to that used by Hooley [3]. The sample was supported with glass wool in a glass tube, which was put in a glass weighing bottle containing the chosen intercalate liquid. A cover glass was quickly placed over the greased open end of the bottle, which had air inside. Time was measured from the moment the sample was introduced in the bottle. The liquid was almost 1 cm high and the sample was about 3 cm above the liquid surface. The edge of the sample was then observed by using a travelling microscope equipped with an X–Y micrometer stage and a digital readout. The system enabled readings to be taken once every 20 s on the average, except for the first reading which was taken after about 40 s from the start. The uncertainty in a single reading was about ± 5 μm. The samples were based on highly-oriented pyrolytic graphite (Grade ZYA) supplied by Union Carbide Corp. and were cut by means of a wire saw into pieces of approximately 7 × 7 mm and were cleaved to thicknesses in the range 0.05 - 0.3 mm.

Bromine, ICl, and HNO_3 were the intercalate species chosen because they are known to cause crack formation in order of increasing severity. A further motivation for the choice of these intercalate species was to investigate the possible effects of the intercalation mechanism on the edge expansion; nitration is known to be accompanied by a progressive change in stage during intercalation to a given eventual stage [8] whereas bromination is not [9].

1.3. Experimental results

1.3.1. Surface profilometry

The sequence of surface profiles obtained at four different times during Br_2 intercalation is shown in Fig. 1. The sample was of diameter 4.5 mm and thickness 0.3 mm. An advancing intercalate front was clearly observed. In the early part of intercalation, the profile was bucket shaped. Later, the profile became V-shaped such that the region outside the V-shaped part of the profile was roughly flat. As intercalation further progresses, the V-shaped part of the profile decreases in size and eventually leaves a rough, flat surface.

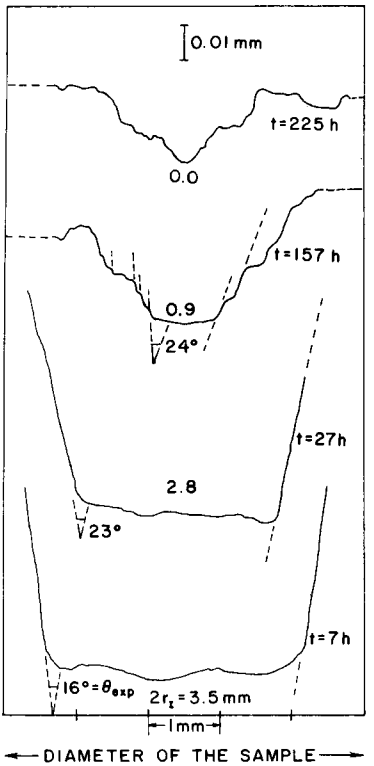

Fig. 1. Sequence of *c*-face surface profiles of a cylindrical HOPG sample (diameter 4.5 mm, thickness 0.3 mm) as bromination proceeds at room temperature.

Of importance is the linearity of the slanted portions of the profile, *i.e.*, the sides of the "bucket". The angle between these sides is indicated for three profiles in Fig. 1. Due to the difference in scale between the vertical and horizontal axes in Fig. 1, the measured angles indicated are not the actual angles. Corresponding to the measured angle θ_{exp} (Fig. 1), the actual slope of the slanted portion is 1/50 cot ($\theta_{exp}/2$). The trend in slope variation, as shown in Fig. 1, is quite representative. This is also shown in Fig. 2, where the actual slope is plotted against the time of intercalation for samples of different diameters and thicknesses. In spite of the scatter in the data points, it is evident that the slope is steep at the beginning and then decreases quickly to a steady value. It should also be noted that the large scatter in the slope data obscures the effect of the size of the sample, if an effect is present. The steady value of the slope is about 0.08. Extrapolation to zero time is quite uncertain, given the time scale shown in Fig. 2.

An interesting feature is the appearance of rings, as seen visually, and of corresponding ledges, as seen in the profiles (*e.g.*, at t = 157 h) in Fig. 1 after some time of intercalation. In many cases, the parallel nature of the ledges is remarkable and simplifies the determination of the slope, as illustrated by the dashed lines in the third profile from the bottom of Fig. 1. The

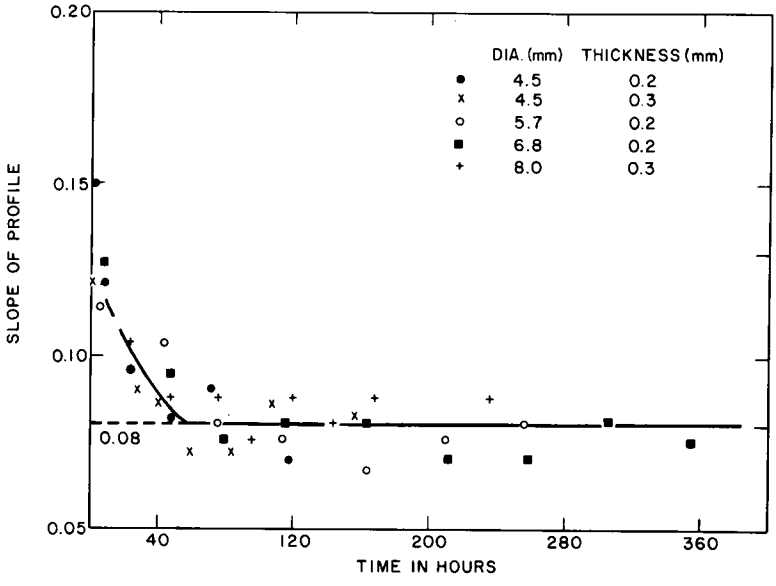

Fig. 2. Plot of the actual slope of the surface profile *vs.* time for samples of various diameters and thicknesses.

number of occurrences of the ledges appears to increase with time, but decrease with increasing sample diameter. Moreover, it is insensitive to the thickness. Although the height of the ledges tends to increase with diameter, the width apparently is independent of size and is of the order of 100 - 150 μm. The origin of the ledges is presently not clear.

The variation in the diameter of the contour of the intercalate front during intercalation is shown in Fig. 3 for samples of different diameters but of the same thickness, and is shown in Fig. 4 for samples of different thicknesses but of the same diameter. The slope of this plot yields the velocity of the front. The general features of the plot are noted below.

(1) Each curve is dominated by a linear portion which indicates that the velocity is constant for the most part of the intercalation process. This means that the intercalation process is interface-controlled. However, the initial portion is characterized by a steeply falling curve, implying that the velocity decreases rapidly from a large, average, initial value ($\sim 5 \times 10^{-6}$ cm/s) to a steady value which is at least an order of magnitude less. The magnitude of the steady velocity is shown for each curve.

(2) Irrespective of diameter or thickness, all the curves approach linearity at approximately the same time ($\sim$44 h), which is close to the time at which the slope becomes steady (Fig. 2). Moreover, the amount of decrease in the intercalate front contour diameter ($\sim$2.3 mm) in this period is apparently independent of the sample diameter or thickness.

(3) There is apparently no correlation between the magnitude of the steady velocity and the sample thickness (Fig. 4). For a given thickness (Fig. 3), the steady velocity appears to be fairly independent of the dia-

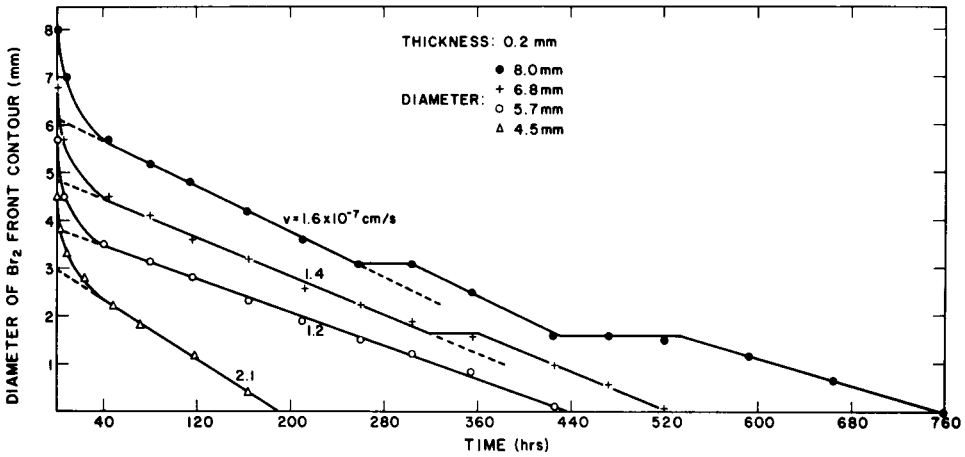

Fig. 3. Plot of the Br_2 front contour diameter *vs.* time for samples of the same thickness but of different diameters. The magnitude of the steady velocity is indicated for each curve.

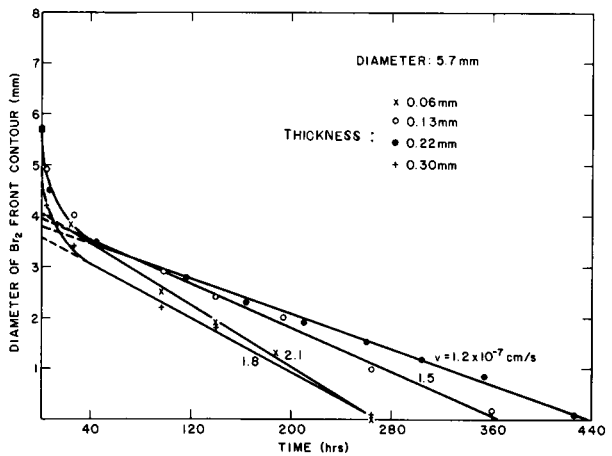

Fig. 4. Plot of the Br_2 front contour diameter *vs.* time for samples of the same diameter but of various thicknesses. The magnitude of the steady velocity is indicated for each curve.

meter, as long as the sample diameter is large compared with ~2.3 mm. However, as the diameter becomes comparable with 2.3 mm, as for the 4.5 mm diameter case, the steady velocity increases with decreasing diameter, though the applicable region decreases in extent.

(4) In Fig. 3, the two curves corresponding to large diameters for the same thickness show "steps" (drawn as a guide to the eyes), whereas the other two curves corresponding to smaller diameters do not. As seen in Fig. 4, for the same diameter, no steps appear as the thickness increases.

An interesting conjecture about the last mentioned feature is that, as the sample diameter increases, the steps may become more numerous so as to

cause considerable decrease in intercalate absorption rate. The step may even assume an indefinite width so that intercalation stops. It is interesting to note contrasting effects of the diameter and thickness found by Hooley [3] in the intercalation of natural graphite flakes of dimensions generally smaller than those used in this work.

The above experimental results were obtained with the sample at room temperature and the bromine vapor pressure at 200 mmHg (corresponding to that in equilibrium with room temperature liquid Br_2). In addition, we have performed surface profilometry for various sample temperatures and various intercalate vapor pressures. With the sample at 22 °C, the speed of intercalation was found to increase with increasing Br_2 vapor pressure; with the Br_2 vapor pressure at 200 mmHg, the speed of intercalation was found to decrease with increasing sample temperature. Shown in Fig. 5 is the variation of the intercalate front position with time during intercalation at various intercalate vapor pressures.

The variation of intercalate vapor pressure provides an investigation of the dependence of the kinetics of intercalation on the final stage. It is also of interest to investigate the dependence of the kinetics of intercalation on the initial stage. All of the results discussed above were obtained with the initial stage being ∞ (*i.e.*, pristine graphite). To investigate the dependence on the initial stage, we have performed surface profilometry during Br_2 intercalation from stage 4 to stage 2. Figure 6 shows the evolution of half of the surface profile during this intercalation. The sample was initially intercalated with the Br_2 vapor pressure at 120 mmHg. X-ray diffraction showed that the compound formed was stage 4, together with a small amount of stage 3. At this vapor pressure, the intercalate front moved at a speed of $v_1 = 9 \times 10^{-8}$ cm s^{-1}. After a certain time period, the Br_2 vapor pressure was changed from 130 mmHg to 200 mmHg, because the compound formed at 200 mmHg is stage 2. A stage 2 compound has a thickness increase of 55% over the pristine graphite, whereas

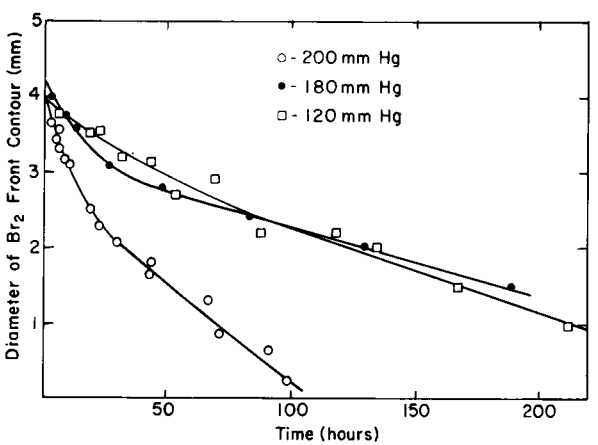

Fig. 5. Plot of the Br_2 front contour diameter *vs.* time for intercalation at different intercalate vapor pressures.

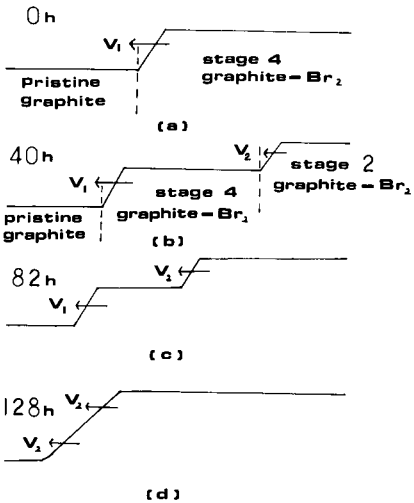

Fig. 6. Schematic diagram showing the evolution of half of the surface profile during two-step intercalation. The first step was vapor phase intercalation at a Br_2 vapor pressure of 130 mmHg, giving stage 4 in the intercalated region. The second step was vapor phase intercalation at a Br_2 vapor pressure of 200 mmHg, giving stage 2 near the edge of the profile. (a) Shows the profile during the first step; (b), (c) and (d) show the second step. $v_1 = 9 \times 10^{-8}$ cm s^{-1}; $v_2 = 2.5 \times 10^{-7}$ cm s^{-1}.

a stage 4 compound has a thickness increase of only 27%. Because of this difference in thickness expansion, the movement of the intercalate fronts of both stage 4 and stage 2 components in the sample could be observed, as shown in Fig. 6(c). The intercalate front of the stage 2 component was found to move at a speed of $v_2 = 2.5 \times 10^{-7}$ cm s^{-1}, while that of the stage 4 component still moved at a speed of v_1. Since $v_2 > v_1$, the stage 2 intercalate front finally caught up with the stage 4 intercalate front and the two fronts became one.

1.3.2. Edge expansion

Figure 7 shows the typical expansion *versus* time curves during the intercalation of the three intercalate species in samples of approximately the same size. In the case of Br_2 intercalation, the expansion approaches a limiting value of 55%, which is indicated by an asterisk in Fig. 8 and is equal to the calculated value, based on X-ray diffraction data, of the lattice expansion. In the cases of ICl and HNO_3 intercalation, the expansion curves exceed the theoretical limits. In particular, nitration caused expansion several times larger than the theoretical limit. This behavior was due to cracks which gradually became visible. In addition, in the case of ICl intercalation, a sharp decrease in the expansion rate characteristically occurred at an expansion corresponding to the theoretical value for a first stage compound. Given a sufficiently thick sample, bromination also causes cracks. Thus, apart from showing the expansion behavior with and without cracks, the comparison of the three curves in Fig. 7 demonstrates that the minimum thickness for cracking, in the presence of saturated intercalate vapor at a

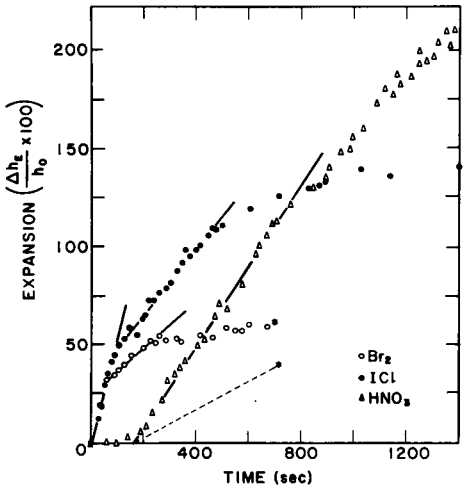

Fig. 7. Variation of the percent. expansion with time during the intercalation of Br_2, ICl, and HNO_3. The theoretical limits in expansion are indicated by *.

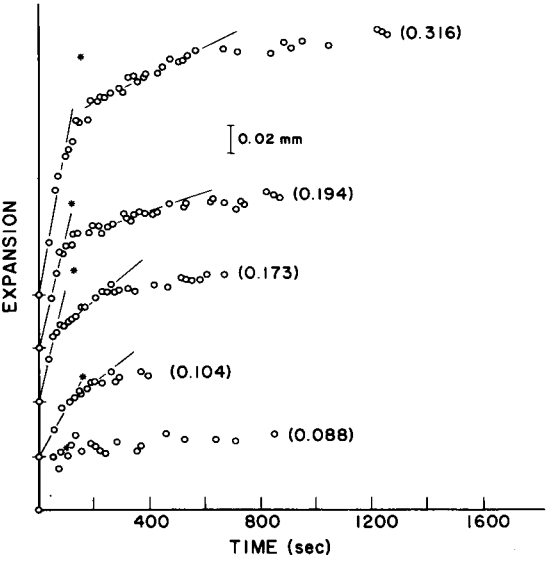

Fig. 8. Variation of expansion with time during Br_2 intercalation of samples of various initial thicknesses, indicated in units of mm in parentheses. The theoretical limits in expansion are indicated by *.

given temperature, decreases in the order Br_2, ICl and HNO_3, as will be expected from comparison of their respective layer spacing expansions d'.

The expansion curves for Br_2 and ICl are rather similar to each other in shape, as expected. For each intercalate, the curve below the theoretical limit, marked by an asterisk in Fig. 7, exhibits two dominant linear portions distinguished by different slopes. This is illustrated in Figs. 8 and 9 with data

for various initial thicknesses. This feature has not been previously reported. The initial slope is always greater than the later one; the ratio seems to increase with the initial thickness in the case of bromination. In fact, the expansion curve for the thinnest sample used (0.088 mm thick) for bromination appeared to be a single, straight line within the experimental uncertainties. Interestingly, the expansion at which the change of slope occurred was neither constant nor a definite fraction of the sample thickness.

The expansion curves for nitration are dominated by an initial linear portion followed by a nonlinear expansion of generally lower expansion rate (Fig. 7). The expansion curve provides no obvious indication of changes in stage during intercalation. Expansion during HNO_3 intercalation differs from that during Br_2 or ICl intercalation by the presence of an "induction period" of about 2 min during which there was no expansion. Previous studies [6, 10] have found that no mass uptake occurred in similar induction periods, though the periods were longer.

On the basis of Hooley's results [1], *i.e.*, that intercalation starts at the *c*-face surfaces and proceeds to the middle of the edge, one would expect the

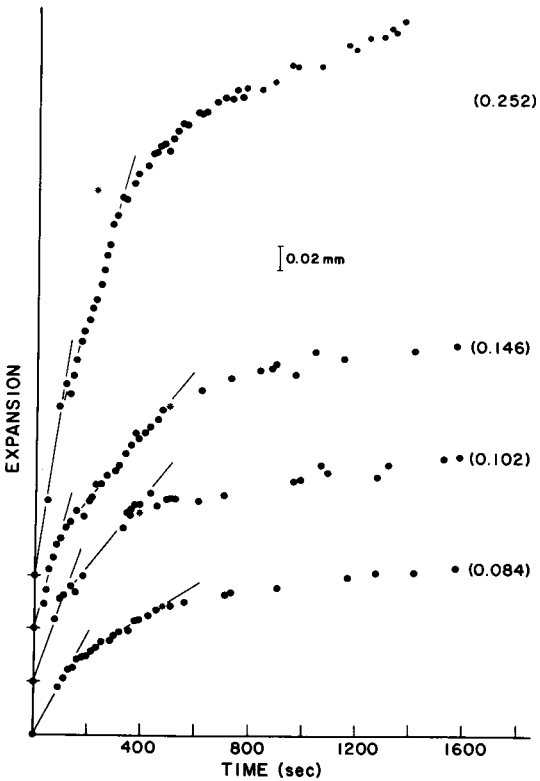

Fig. 9. Variation of expansion with time during ICl intercalation of samples of various initial thicknesses, indicated in units of mm in parentheses. The theoretical limits in expansion are indicated by *.

absolute expansion rate to be independent of sample thickness. As shown in Fig. 10, we observed that the absolute expansion rate increased with sample thickness for all three intercalate species. Furthermore, the surface cracks which appeared at early stages of ICl and HNO_3 intercalation showed no spacial preference and were distributed uniformly over the graphite surface. Both of these observations suggest that intercalation is initiated uniformly over the graphite surface. The disagreement with Hooley's results probably is due to the much thicker specimens used by Hooley than those examined in this work.

1.4. Model of interface-controlled intercalation

The proposed model is based on a mechanism of nucleation and subsequent growth, considered for simplicity in a perfect graphite structure.

According to the mechanism suggested by Hooley [1] for the intercalation of bromine in graphite, we assume that intercalation starts at the interlayer spaces at the two ends and proceeds toward the inner region in such a way that there are n graphite layers between two successive, nucleated intercalate layers for an eventual n-th stage intercalation compound*. We further assume that the nucleation of an intercalate layer occurs at the edge of the layer, and that once nucleated, the intercalate layer grows toward the inside at a velocity, v, which is, in general, a function of time. The structure of the resulting intercalate layer corresponds to that of an n-th stage compound. As the first intercalate layer grows, nucleation occurs at the inter-

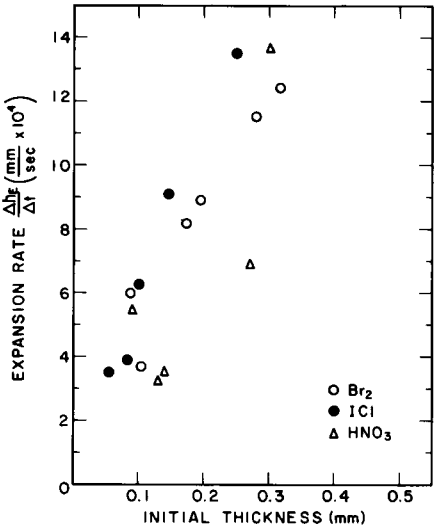

Fig. 10. Dependence of the absolute expansion rate on the initial thickness.

*This assumption implies that the system does not progressively go through different stages on the way to a given stage.

layer space separated by n graphite layers from the first intercalate layer. In this way, the nucleation and growth of an intercalate layer eventually take place at every interlayer space appropriate for the n-th stage compound. Let the time gap between the nucleation of two successive intercalate layers be ΔT, which we assume to be constant at a given pressure and temperature.

A schematic diagram of a sample at an instant of time during intercalation to a stage 2 compound is shown in Fig. 11. When the intercalate enters an interlayer space, it forces the spacing between the bounding graphite layers to expand. Thus, the thickness profile as well as the weight of the sample change as intercalation proceeds. On the basis of the above model, these changes can be expressed analytically as functions of the time of intercalation. For simplicity, we have restricted our consideration to cylindrical samples with the thickness along the c-direction, though the analysis can be extended to samples of other shapes. Let the radius of the cylinder be R_0; let there be Nn graphite layers in the cylinder, where n is the stage of the compound that eventually forms. This means that the number of intercalate layers in the cylinder after the completion of intercalation is N. The thickness of the cylinder before intercalation is Nnd, where d is the interlayer spacing in pure graphite.

The proposed model indicates the existence of several time lengths that are of importance. Let the time taken for the nucleation of all intercalate layers be t_N, which is given by

$$t_N = \left(\frac{N}{2} - 1\right) \Delta T \approx \frac{N}{2} \Delta T \tag{1}$$

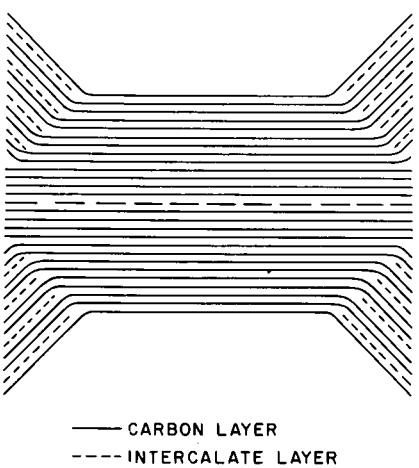

Fig. 11. Schematic diagram of a sample at an instant of time during intercalation to a stage 2 compound.

The above approximation is used in the rest of this model.

Let $r(t) = R_0\, g(vt/R_0)$ denote the radius of the advancing (inner) front of an intercalate layer at time t after its formation. If the layer grows at a steady velocity, v, g is simply given by

$$g\left(\frac{vt}{R_0}\right) \equiv 1 - \frac{vt}{R_0} \,. \tag{2}$$

In what follows, each intercalate layer is assumed to grow with the same velocity, v, in the manner described by eqn. (2). The radius of the intercalate front contour for the j-th intercalate layer at time t is given by

$$r_j = R_0 - v(t - j\Delta T) \,. \tag{3}$$

Clearly, the time of completion of growth of the outermost layers is $t_G = R_0/v$. The time when intercalation is finished corresponds to the time at which the $N/2$-th intercalate layer (the middle intercalate layer) completes its growth. This occurs at a time $t_I = t_N + t_G$ after the start of intercalation.

Depending on the ratio of the thickness to the radius of the cylindrical sample at a given pressure and temperature, one of two cases occurs during intercalation.

Case 1: $t_N \leqslant t_G$.

This means that the nucleation of all intercalate layers is completed before the growth of the outermost layers is completed.

Case 2: $t_N \geqslant t_G$.

This means that the nucleation of intercalate layers continues after the growth of the outermost layers is completed.

1.4.1. Surface profile

To follow the variation in the surface profile during intercalation for Case 1, consider, separately, three time intervals: (a) $0 \leqslant t \leqslant t_N$, (b) $t_N \leqslant t \leqslant t_G$ and (c) $t_G \leqslant t \leqslant t_I$.

Consider first the interval $0 \leqslant t \leqslant t_N$. Let $h(r,t)$ be the increase in thickness at a distance r from the center and at a time t from the start of intercalation. Note that, for a cylindrical sample, the intercalate front is circular, so that h is radially symmetrical.

Let us assume that the increase in the separation of two consecutive graphite layers at r is proportional to the concentration at r of the intercalate layer in between them. In interface-controlled intercalation, there is no intercalate concentration gradient in the intercalated region. Thus, half of the total increase in thickness is given by

$$h(r,t) = d'j, \tag{4}$$

where $2j$ is the number of intercalate layers that have progressed up to point r at time t, and d' is the change in the spacing between two adjacent graphite layers due to the insertion of an intercalate layer in between (3.7 Å for Br_2

intercalation). Putting eqn. (4) in eqn. (3) yields the equation for the thickness at r for $t \leqslant t_N$:

$$r = R_0 - v\left(t - \frac{h\Delta T}{d'}\right). \tag{5}$$

The intercalate front corresponds to $h = 0$ in eqn. (5) and its position $r = r_I$ is given by:

$$r_I = R_0 - vt. \tag{6}$$

Rearrangement of eqn. (4) gives

$$h(r,t) = \begin{cases} \dfrac{d'}{v\Delta T}\left[r - (R_0 - vt)\right], & r \geqslant r_I \\ 0, & r \leqslant r_I. \end{cases} \tag{7}$$

Before intercalation begins ($t \leqslant 0$), the profile is flat, as shown by curve 0 in Case 1 of Fig. 12. As time progresses, the profile corresponding to eqn. (8) on one of the c-faces becomes bucket-shaped, as indicated by the line abcd (curve 1) in Case 1 of Fig. 12. The slanted linear portions (ab, cd) have a slope equal to $d'/v\Delta T$ and the intercalate front (b, c) moves with a constant velocity equal to v. As intercalation proceeds further, the straight lines ab or cd translate parallel to themselves toward the center.

The edge thickness increases to the maximum value, $h_\infty = Nd'$, at a time $t = t_N$. After time $t = t_N$, the lines ab and cd continue to translate parallel to

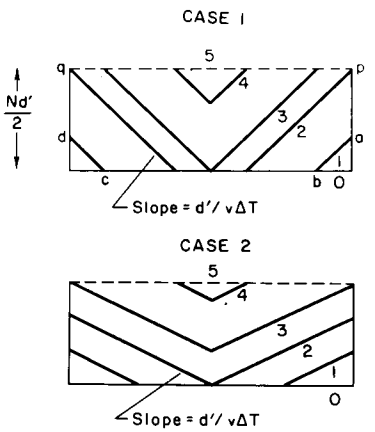

Fig. 12. Schematic diagram of the sequence of surface profiles as interface-controlled intercalation proceeds with time.
Case 1 ($t_N \leqslant t_G$). Curve 0: $t = 0$; 1: $t < t_N$; 2: $t = t_N$;
3: $t = t_G$; 4: $t > t_G$; 5: $t = t_I$;
Case 2 ($t_N \geqslant t_G$). Curve 0: $t = 0$; 1: $t < t_G$; 2: $t = t_G$;
3: $t = t_N$; 4: $t > t_N$; 5: $t = t_I$.

themselves until time $t = t_G$, when these lines meet at the center of the sample and result in a V-shaped profile, as shown by curve 3 in Case 1 of Fig. 12. At this time, the formation of the first intercalate layers is completed. After this, the V-shaped part of the profile becomes smaller as more intercalate layers are completely formed, as shown by curve 4 in Case 1 of Fig. 12. When intercalation is completed ($t = t_I$), the V-shaped part of the profile vanishes, leaving a flat surface, as shown by the line pq (curve 5) in Case 1 of Fig. 12. This line is parallel to line bc and is at a height of $Nd'/2$ from line bc.

Similar arguments give the evolution of the surface profile for Case 2 ($t_N \geqslant t_G$), as illustrated in Fig. 12.

The evolution of surface profiles as predicted for Case 1 of the model of interface-controlled intercalation is in excellent qualitative agreement with the experimental results in Fig. 1. In particular, the change of a "bucket" shape to a "V" shape, as discussed in the model, is well confirmed. All experimental results belong to Case 1, in which the time of nucleation of all layers (t_N) is less than the time of completion of the outermost layers. This is not unexpected in view of the fact that the samples used had the thickness much less than the diameter.

As indicated already in Figs. 2 - 4, the slope of the profiles and the velocity of the intercalate front remain constant for the most part of the growth period, as was assumed in the model. However, the initial period is apparently marked by changing slope and velocity. This can possibly be attributed to an edge effect for the following reasons. The fact that the velocity decreases from a large value at the edge to a smaller, steady value after the intercalate layers have moved a certain distance inside the sample is consistent with a smaller resistance to deformation at the edge than inside. Moreover, the distance the intercalate front moves inside until the steady state is reached is independent of the sample diameter. This means that steady state can be considered to correspond to an infinite sample.

Since, in the model, the slope is equal to $d'/v\Delta T$, where d' is the expansion of the graphite layer spacing and ΔT is the time gap between the formation of two successive intercalate layers, it might seem that the initial decrease in slope may be explained by an increase in ΔT with time. However, the explanation might be applied only up to time t_N, which is also the time required for completing the edge expansion. For the HOPG samples used in the present work, t_N is of the order of a few minutes, as determined by edge expansion measurement (Section 2.4.2), whereas the slope continues to decrease for a much longer time (~44 h). Alternatively, the simple assumption of constant ΔT, with the velocity of growth of the intercalate layers decreasing with increasing distances from the surfaces, can explain the decrease in slope. Indeed, it is quite reasonable to assume that the further away from the c-face surface an intercalate layer is, the smaller is the velocity due to the increasing rigidity until the steady state is reached. Since the time of the first measurement is a few hours after the start of intercalation, a rigorous determination of the parameter ΔT used in the model cannot be made. This is because the determination of ΔT requires the evaluation of the

slope by extrapolation to zero time. Due to the scatter in the data, this extrapolation is quite rough. However, this difficulty does not necessarily exist in the case of samples which have large values of t_N. It must be noted that using the value of the steady slope yields only a redefined value of ΔT, which is about 3 s, as compared with the value of 10^{-3} s obtained from edge expansion results.

1.4.2. Edge expansion

It follows from eqn. (7) that at the edge, where $r = R_0$ the total expansion $h_E = 2h$ is given by

$$h_E(t) = \begin{cases} 2d' \dfrac{t}{\Delta T}, & 0 \leqslant t \leqslant 1/2(N\Delta T) \\ \\ Nd', & t \leqslant 1/2(N\Delta T). \end{cases} \tag{8}$$

Edge expansion is finished when all the intercalate layers are nucleated, *i.e.*, at a time equal to $1/2(N\Delta T)$. Thus the model predicts that the expansion is linear in time and that ΔT is inversely proportional to the rate of expansion.

The edge expansion results obtained during Br_2 and ICl intercalation can be described fairly well by the model if the quantity ΔT is allowed to increase to a larger value after some expansion. This appears plausible because the middle layers may be constrained in such a way as to cause a change in the rate of nucleation. Let ΔT_1 be the value of ΔT corresponding to the first slope; let ΔT_2 be the value of ΔT corresponding to the second slope. The ratio of ΔT_2 to ΔT_1 is always equal to, or greater than, unity, as mentioned earlier. Considered in the light of the model, the graphite (natural flakes)–$FeCl_3$–nitromethane system investigated in detail by Hooley [3] seems to provide an interesting example of a situation in which ΔT_2 is infinite; *i.e.*, there is no further expansion. The data indicate that the edge expansion of the flakes is initially quite linear in time and then it stops at an expansion which is generally less than the maximum possible. However, there is a difference between the $FeCl_3$ intercalation of Hooley and our Br_2 and ICl intercalation in that the initial rate of expansion appears to decrease with increasing initial thickness in the case of the former, whereas the opposite is true for the latter. For comparable thicknesses, ΔT_1 for $FeCl_3$ intercalation is of the order of 0.1 s, which is about two orders of magnitude greater than the corresponding value for Br_2 or ICl intercalation. This is not surprising in view of the low molarity of $FeCl_3$ in the $FeCl_3$–nitromethane solution used.

The sensitivity of ΔT_1 to the partial pressure of an intercalate at a fixed temperature can be seen in Fig. 13, when $\log \Delta T_1$ is plotted against $p_o/(p - p_{th})$, where p_o is the vapor pressure of Br_2 at the fixed temperature, p is the Br_2 pressure and p_{th} is the threshold pressure. The ΔT_1 values were calculated using eqn. (8) from the data obtained by Saunders *et al.* [5] with

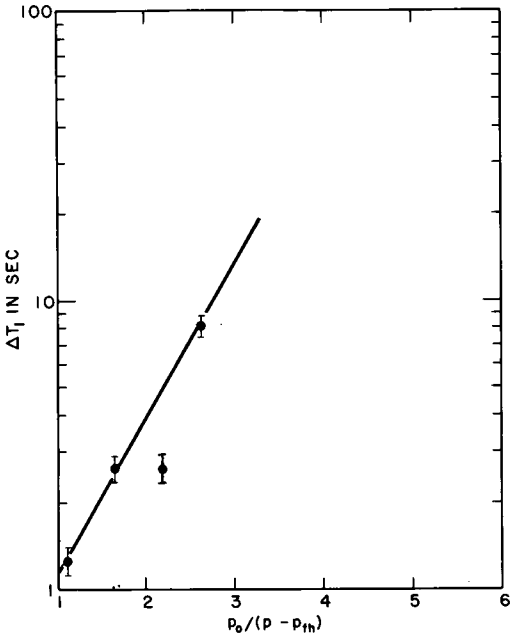

Fig. 13. Log ΔT_1 *vs.* $p_o/(p - p_{th})$, where p_o is the vapor pressure of Br_2 at the fixed temperature, p is the Br_2 pressure and p_{th} is the threshold pressure.

an uniaxial load on the sample at 20 °C. On the basis of the linearity of the plot, which is based on limited data points, the dependence of ΔT_1 on Br_2 pressure, p, may be written in the following empirical form:

$$\Delta T_1 = A \exp [B/(p - p_{th})] (p \geqslant p_{th}), \tag{9}$$

where A and B are functions of temperature. In Fig. 13, p, corresponding to a certain mole fraction of Br_2 in the Br_2–CCl_4 solution, was obtained from the table in ref. 6. At $p = p_{th}$, ΔT_1 is infinite, indicating that no intercalation takes place. For the case of pure bromine, Fig. 13 shows that $\Delta T_1 = 1.2$ s, which is very large compared with the first value given in Table 1. This is due to the fact that a load of 95 kg/cm^2 was applied to the sample in the work of Saunders *et al.* [5].

The perfection of the graphite material also has a large influence on the rate of expansion or ΔT_1, as shown in Table 1, where the samples are listed in order of increasing perfection of the graphite material. In particular, the results of Hooley *et al.* [5] on samples of equal thickness clearly show the trend that the higher is the perfection of the graphite material, the smaller is ΔT_1 or the higher is the rate of expansion. A similar trend applies to the electrical resistivity and threshold pressure [11]. In the absence of sufficient relevant data, it is difficult to establish an absolute correspondence between ΔT_1 and the variables mentioned above. However, ΔT might prove to be equally as good as resistivity or threshold pressure in determining the per-

TABLE 1

Values of ΔT_1 for intercalation of different types of graphite at a Br_2 pressure of 145 mmHg at 20 °C

Source	*Sample*	*Dimensions* * (cm)	ΔT_1 (s)
Saunders *et al.* [5]	A	0.4 × 0.4 × 0.1	7×10^{-2}**
Hooley *et al.* [1]	PG1	0.26 (dia.) × 0.6	1.9×10^{-2}***
	PG3	0.26 (dia.) × 0.6	4.2×10^{-4}***
	PG6	0.45 × 0.45 × 0.6	1.5×10^{-4}***
Present work	HOPG	0.7 × 0.7 × 0.03	6.8×10^{-4}

*The last dimension listed is the thickness.

** This value is obtained by extrapolating the curve of ΔT_1 *vs.* load at 20 °C, to zero load.

***These values are based on the data given in Table 1 of ref. 1; they are rough estimates only. Disc production tends to underestimate the values by enhancing the rate of expansion.

fection of the graphite material, especially since ΔT_1 has the advantage of being easily measurable. However, ΔT_1 has the disadvantage of being dependent on the size, particularly the thickness, as shown by comparison of the data in the last two lines in Table 1. ΔT_1 for HOPG is expected to be smaller than that for PG6, but, due to a difference in thickness, it is not.

The stage of an intercalation compound is best determined by X-ray diffraction. The stage number as well as the layer spacing expansion should ideally agree with the macroscopic expansion along the *c*-axis. Conversely, the stage number can ideally be ascertained from the macroscopic expansion [12] with the help of only the knowledge of the layer spacing expansion. From eqn. (8), the theoretical maximum macroscopic expansion is Nd'. The initial thickness can be written as Nnd, where n is the stage number and d is the pure graphite layer spacing (3.35 Å). Thus, the theoretical fractional expansion is d'/nd. For the first stage ($n = 1$) graphite–ICl compound, $d' =$ 3.89 Å, so that the theoretical fractional expansion is 116%, as indicated by asterisks in Fig. 9. It is clear that the presence of cracks will lead to misleading results, as is evident in the review of different previous results for ICl intercalation [13]. Therefore, measurement of the final expansion is not as revealing as that of the expansion during the whole course of intercalation.

The model is applied to nitration by assuming that ΔT_1 is an overall rate determining quantity, since an initial linear portion is obtained in the experimental data of expansion *vs.* time (Fig. 6). We further assume that the time at which the lattice expansion is finished corresponds to the time when the curve deviates from linearity in Fig. 6. In this context, the dashed line in Fig. 6 represents the true lattice expansion. It should be mentioned that the concentration of fuming nitric acid used in this work was such that a third stage graphite nitrate resulted, as verified by X-ray diffraction. Accordingly, ΔT_1 for nitration is 8.0×10^{-3} s.

There has not been much experimental data which can yield clues to the relationship between ΔT_1 and temperature. From the data of Saunders *et al.* [5], it is evident that the rate of expansion falls with increasing temperature. This is consistent with the fact that the velocity of the intercalate front decreases with temperature (Section 2.3.1) and with the interpretation of ΔT given in terms of the velocity (Section 2.4). If the distance an intercalate layer has to move inward before the next layer is nucleated does not vary much with temperature, the decrease in velocity means a longer time gap (ΔT_1) between successive nucleation events. The threshold pressure also increases with temperature [4, 5]. This is not unexpected if we assume that the threshold pressure represents the pressure for the initiation of nucleation.

The decrease in the expansion rate during Br_2 intercalation is consistent with the discrepancy found in the later period of expansion between the model prediction and the experimental curve of fractional expansion *vs.* fractional mass uptake (Section 2.4.3). The calculated curve based on a single ΔT rises faster than the data beyond 80% of the expansion. Taking into account a slower rate of expansion will obviously reduce the discrepancy. It may be noted that the stage number n need not be an integer as has been tacitly implied in the model. In fact, n can be defined just as the ratio of the number of graphite layers to the number of intercalate layers. This is in accordance with the finding that the equilibrium expansion under a certain pressure is proportional to the mass uptake [4, 5]. A similar view has also been adopted in connection with the interpretation of X-ray diffraction patterns [14]. This, of course, means that ΔT should be considered as an average time gap between two successive nucleation events.

2. Kinetics of desorption

Desorption is due to the thermodynamic instability of lamellar compounds. This instability results from the relatively weak bonding between carbon and the intercalate and between adjacent intercalate atoms or molecules, as evident in graphite–Br_2. Surface profilometry, described in Section 2.1, has been performed to study the kinetics of desorption, with further information obtained through isothermal and scanning thermogravimetry, as well as detecting the effluent gas during desorption.

2.1. Experimental techniques

2.1.1. Gas detection

The detection of desorbed intercalate from a sample upon heating was achieved by using an effluent gas analyzer incorporated in a differential scanning calorimeter (Perking-Elmer DSC-1B). The analyzer consisted of a two-thermistor bridge circuit which monitored the thermal conductivity of the DSC sample holder purge gas relative to the gas which bypassed the sample holder. The system was purged at 30 cm^3/min with dry nitrogen. A weighed graphite–Br_2 sample was placed in a platinum pan and mounted in

the DSC sample holder which was purged for about 10 min at room temperature. The sample temperature was increased at either 5 or 10 °C/min. A Columbia Scientific Industries integrator was used to record the effluent analyzer output; the acquisition rate was 5 or 10 per min.

2.1.2. Thermogravimetry

The thermal gravimetric measurement was performed by using a Perkin-Elmer electronic microbalance (Autobalance Model AD-2Z), which has a maximum sensitivity of 0.1 μg. The sample was placed on a pyrex pan which was suspended by a pyrex hangwire. A 19 mm i.d. pyrex tube enclosed the hangwire and the sample pan. During the measurement, the tube was slowly purged with argon at approximately 20 cm^3/min. A low mass furnace surrounded the sample pan and was controlled by a Theall Engineering Model TP-2000 temperature programmer, which was capable of either isothermal or scanning temperature control. The sample temperature was measured by placing a chromel–alumel thermocouple immediately below (within 2 mm) the sample pan. During isothermal measurements, the controller kept the sample temperature within 1 °C from the programmed temperature. All temperature scans were performed at a heating rate of 2 °C/min.

2.2. Experimental results

2.2.1. Gas detection

Typical effluent gas analyzer response is shown in Figs. 14 and 15. A graphite–Br_2 sample, which had been allowed to desorb at room temperature from 83 to 43.3 wt.% Br_2, was heated from room temperature to 107 °C at 10 °C/min, as shown in Fig. 14. Little evolved bromine was detected until 101 °C. At this point a considerable amount of intercalate was detected and is interpreted as being an effect of intralayer intercalate position disordering at 100 °C.

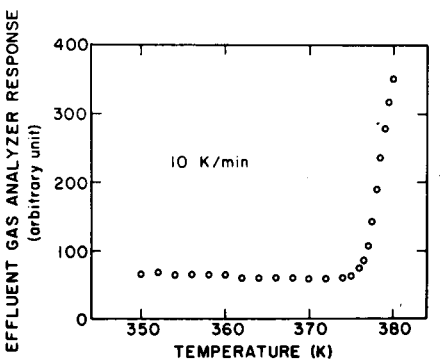

Fig. 14. Effluent gas detector response as a function of temperature, showing desorption commencing at the intralayer order–disorder transformation temperature in graphite–Br_2 (100 °C). The sample contained 43.3 wt.% Br_2 before heating.

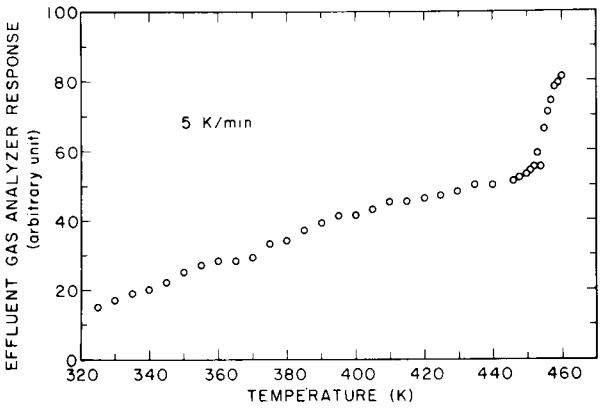

Fig. 15. Effluent gas detector response as a function of temperature, showing desorption associated with exfoliation near 177 °C. The sample contained 21.5 wt.% Br_2 before heating.

Figure 15 shows the effluent gas analyzer response for a less concentrated graphite–Br_2 sample at a higher temperature range and sensitivity. The sample was originally a saturated lamellar compound (83 wt.% Br_2); prior to this temperature scan, it had been desorbed at room temperature and by heating to about 117 °C, and it contained 21.5 wt.% Br_2. The temperature of the sample was scanned from room temperature to 187 °C at 5 °C/min. In Fig. 15, the analyzer trace increases slowly (probably due to baseline drift at this high sensitivity) until about 177 °C, where the amount of desorbed intercalate increased sharply. This increase is attributed to extensive exfoliation, which was visually confirmed at 176 °C for this sample.

The amount of vapor desorbed near 101 °C has been found to increase significantly with increasing intercalate concentration. At low intercalate concentration, as for the sample of Fig. 15, this increase at ~102 °C was too small to be observed, By contrast, at relatively high intercalate concentrations, as for the sample of Fig. 14, a large increase was observed at ~102 °C.

By using the gas detection technique, we have found that the intralayer order–disorder transformation and exfoliation greatly affect the rate of intercalate desorption. However, the effect of the order–disorder transformation on desorption is small at low intercalate concentrations. In order to study these effects more precisely and to obtain information on the kinetics of intercalate desorption, we have used thermogravimetry, as described in Section 2.2.2.

2.2.2. Thermogravimetry

2.2.2.1. Isothermal desorption. Isothermal desorption was studied on graphite–Br_2 prepared by exposing pristine, highly-oriented pyrolytic graphite (HOPG) to bromine vapor at room temperature for a sufficient amount of time to produce saturated stage 2 graphite–Br_2 (83 wt.% Br_2). The sam-

ples were approximately 4 × 4 × 0.5 mm in size and weighed between 9 and 18 mg before intercalation. The uncertainty in sample weight was ± 10 μg.

Figure 16 shows the intercalate concentration (in wt.% Br_2) as a function of time for samples desorbed at 50, 60, 70, 80 and 90 °C. During the early part of the desorption process, the desorption rate increases as the temperature increases. However, complete desorption does not occur, as a significant portion of the original intercalate (~19 wt.% of parent graphite) is retained by the parent graphite even after a long desorption time. This behavior is clearly shown by the 90 °C desorption curve. In a similar manner, samples desorbed at lower temperatures also approached this minimum concentration, given sufficient time. Since ~19 wt.% Br_2 is strongly retained by the graphite at these temperatures (for desorption below 100 °C), this amount is subtracted from the total amount intercalated to yield the "desorbable" portion of the intercalate. The weight fraction of desorbable intercalate remaining is thus defined as

$$\frac{M}{M_\infty} = \frac{M - M_\infty}{M_0 - M_\infty}, \tag{10}$$

where M_0 is the mass of intercalate before desorption, M_∞ is the mass of intercalate after an infinitely long desorption time, and M is the instantaneous mass of intercalate.

Desorption curves for desorption at temperatures above the intralayer order–disorder transformation temperature are shown in Fig. 17. Due to the anomalously high desorption rate at the intralayer order–disorder transformation temperature, it was impossible to maintain a high intercalate concentration above the order–disorder transformation temperature. As a result, measurements above the order–disorder transformation temperature could only be performed on relatively dilute compounds. The temperatures chosen for the isothermal measurements were 110, 120, 130 and 140 °C. As shown in Fig. 17, desorption at these temperatures led to intercalate concentrations less than 18 wt.% Br_2. However, the minimum concentration has not been determined and the effect of the order–disorder transformation on the con-

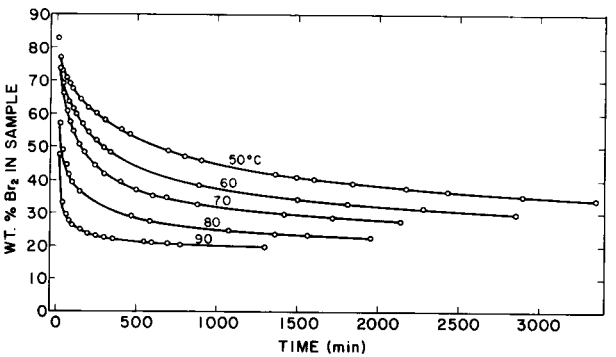

Fig. 16. Isothermal desorption curves of initially saturated graphite–Br_2 at temperatures below the intralayer order–disorder transformation temperature.

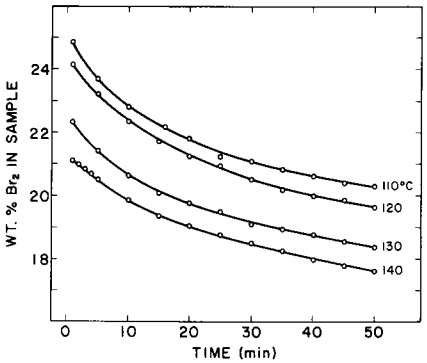

Fig. 17. Isothermal desorption curves of relatively dilute graphite–Br_2 at temperatures above the intralayer order–disorder transformation temperature.

centration has not been quantitatively studied. Nevertheless, like desorption below the order–disorder transformation temperature, the desorption rate above the order–disorder transformation temperature increases as the temperature increases.

2.2.2.2. Scanning thermogravimetry. Because the desorption rate is very high at high temperatures for high concentration samples, measurement during temperature scanning was performed on samples of starting concentration less than 30 wt.% Br_2. The uncertainty in the sample weight was ± 10 μg at low temperatures and increased as the temperature increased, since disturbance caused by violent desorption or exfoliation occurred at high temperatures.

Figure 18 is a plot of intercalate concentration *vs.* temperature for three samples which were obtained by desorbing saturated graphite–bromine compounds at various temperatures, to the starting concentration. The samples were heated at 2 °C/min, and held isothermally at 120, 130, or 140 °C for 50 min before being heated to higher temperatures. The sample associated with curve 1 was initially desorbed at 60 °C and was held at 120 °C. The samples yielding curves 2 and 3 were desorbed at 50 and 70 °C, respectively, and were held at 130 and 140 °C, respectively.

As shown in Fig. 18, the sample weight decreases sharply at two distinct temperatures. The first decrease occurs at approximately 98 °C and corresponds closely to the temperature associated with the intralayer intercalate position order–disorder transformation. The desorption rate below this temperature is negligible compared with that above this temperature. The second decrease occurs at ~165 - 170 °C and is associated with exfoliation. The desorption rate and the equilibrium intercalate concentration above the exfoliation temperature have not been determined in this work. However, it was observed that the sample weight did not decrease smoothly but jumped, indicating perhaps that desorption above the exfoliation temperature occurred in spurts. Moreover, the exfoliation temperature appeared to depend on the desorption temperature prior to the temperature scan, such that the lower

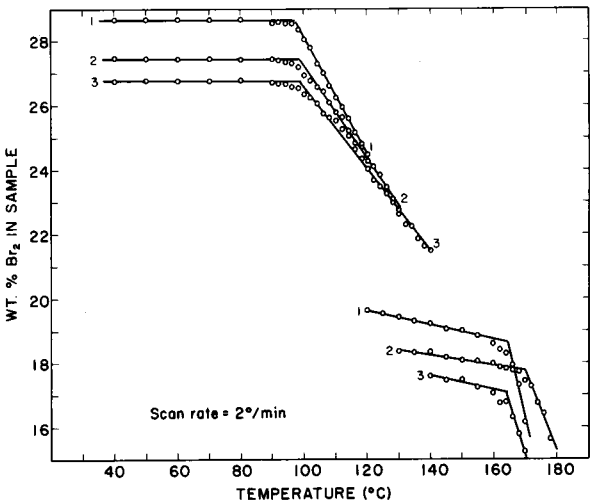

Fig. 18. Scanning thermogravimetric curves taken at 2 °C/min for three relatively dilute graphite–Br_2 samples. The scan was interrupted for 50 min at 120 °C for Sample No 1, at 130 °C for Sample No. 2, and at 140 °C for Sample No. 3.

the initial desorption temperature, the higher the exfoliation temperature. These observations on exfoliation are consistent with our thermal mechanical analysis results [15].

2.3. *Discussion*

2.3.1. *Model of desorption*

We propose to model the desorption process as out-diffusion of the intercalate. The intercalate concentration $C(x,t)$ is assumed to be uniform throughout the sample prior to desorption ($t \leqslant 0$). Let

$$C(x,0) = C_0 \,, \tag{11}$$

i.e., C_0 is the initial intercalate concentration. The out-diffusion process is governed by the continuity equation

$$\frac{\partial C}{\partial t} = D\frac{\partial^2 C}{\partial x^2} \,. \tag{12}$$

To simplify the solution, the sample is assumed to be infinitely large along the x-axis. This gives the boundary condition

$$C(\infty, t) = C_0 \,. \tag{13}$$

If D is assumed to be constant, eqn. (12) can be solved to give

$$\frac{C(x,t)}{C_0} = \mathrm{erf}\left(\frac{x}{2\sqrt{Dt}}\right). \tag{14}$$

Equation (14), in turn, can be used to determine the weight fraction of desorbing species remaining as ref. 16

$$\frac{M}{M_\infty} = \left(\frac{2Dt}{\pi l^2}\right)^{1/2} \tag{15}$$

where t is the desorption time, D is the diffusion coefficient and l is the width of the sample [16]. The sample is of finite size, so the boundary condition expressed in eqn. (13) does not hold exactly. However, this boundary condition can be assumed in the beginning of the desorption process and eqns. (14) and (15) are applicable.

Since the thickness of an intercalation compound is proportional to the concentration, eqn. (14) also indicates the c-face surface profile during desorption. Figure 19 shows the evolution of the concentration profile along the c-face according to eqn. (14). The experimental c-face surface profiles shown in Fig. 20, obtained during room temperature desorption in air of $C_{16}Br_2$ based on HOPG, are in qualitative agreement with those predicted in Fig. 19. In contrast to intercalation, no sharp intercalate front was observed during desorption.

Figure 21 is a plot of ln D *vs.* $1/T$, where D is determined by the initial slope of the M/M_∞ *vs.* $(t/l^2)^{1/2}$ curves shown in Figs. 22 and 23. If the diffusion coefficient is written as

$$D = D_0 \exp\left(-\frac{E_D}{RT}\right), \tag{16}$$

where E_D is the activation energy (per mol) for diffusion, the slope of a plot of ln D *vs.* $1/T$ is equal to $-E_D/R$. By this relation the activation energy for diffusion is found to be 17 kcal/mol below 100 °C, the order–disorder transformation temperature, and 4 kcal/mol above the order–disorder transformation temperature. The value of 17 kcal/mol is in agreement with the 11 - 14 kcal/mol activation energy determined by Aronson [17] for the self-dif-

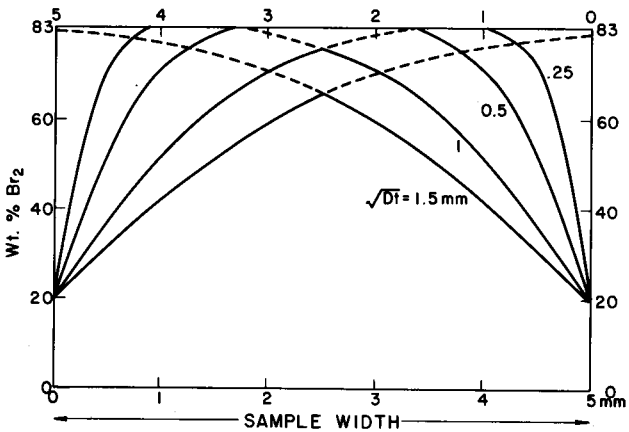

Fig. 19. Evolution of the concentration profile along the c-face according to the proposed model of desorption.

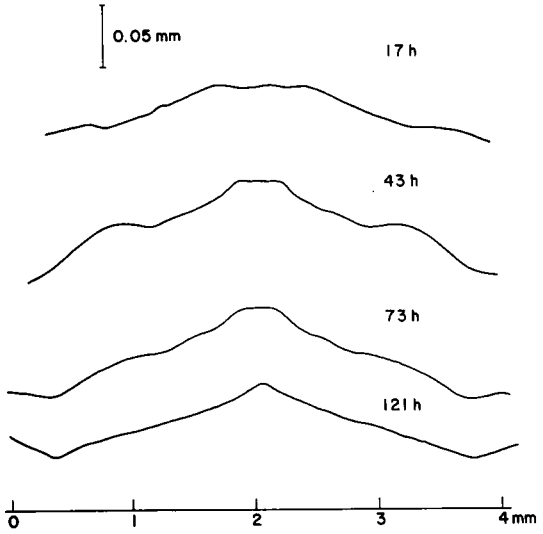

Fig. 20. Experimental *c*-face surface profiles obtained at different times during room temperature desorption in air of $C_{16}Br_2$ base on HOPG.

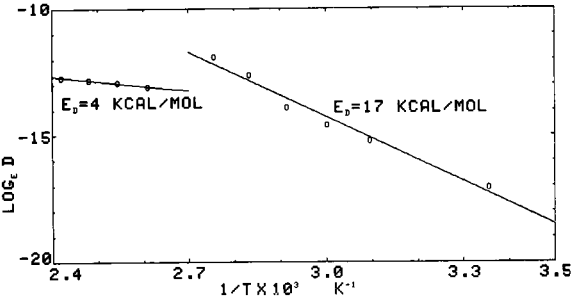

Fig. 21. A plot of ln D *vs.* $1/T$, where D is determined by the initial slope of the M/M_∞ *vs.* $(t/l^2)^{1/2}$ curves shown in Figs. 22 and 23.

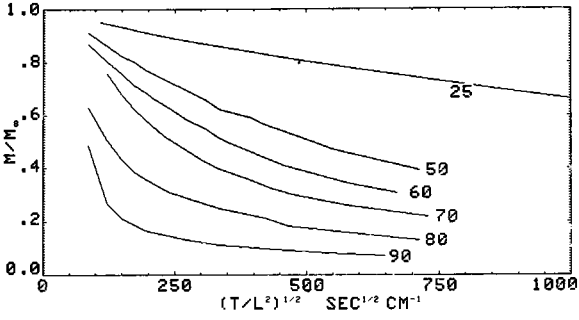

Fig. 22. A plot of M/M_∞ *vs.* $(t/l^2)^{1/2}$ for desorption at temperatures below the intralayer order–disorder transformation temperature of graphite–Br_2.

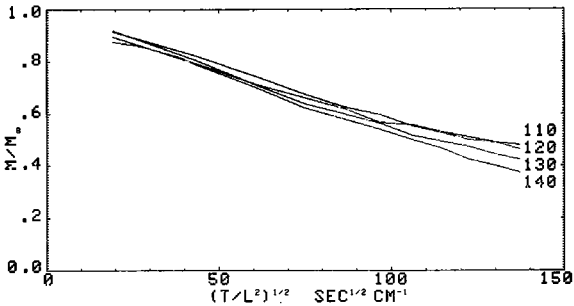

Fig. 23. A plot of M/M_∞ *vs.* $(t/l^2)^{1/2}$ for desorption at temperatures above the intralayer order–disorder transformation temperature.

fusion of bromine within an intercalate layer in the temperature range 30 - 50 °C. The lower activation energy above the order–disorder transformation temperature is consistent with the intuitive notion that diffusion should be easier in a disordered material. For example, the activation energy for diffusion in a liquid is lower than in a solid. In the case of β-brass [18], the activation energy for diffusion is lower in the high temperature β than in the ordered β'.

As the concentration of bromine within a layer is apparently independent of stage, a bulk concentration gradient indicates a succession of stages. As the diffusion coefficient within a layer is likely to be constant, and interlayer diffusion is unlikely, the flux through a given area should be related to the stage in that area, that is, the bulk diffusion coefficient should be concentration dependent, perhaps inversely proportional to the stage number. While M/M_∞ would still be proportional to $t^{1/2}$ at short times, such a concentration dependence would cause increasing deviation from proportionality as desorption progresses, as is evident in Fig. 22. Such a dependence is also indicated by the diffusion coefficients measured above the order–disorder transformation temperature. To avoid exfoliation the high temperature samples were desorbed to a nominal concentration of 28 wt.% Br_2 at room temperature before being heated and weighed at high temperatures. Consequently, the diffusion coefficient can be smaller at high temperatures though the activation energy is less at these temperatures.

3. Conclusion

The kinetics of intercalation and desorption have been studied by following the physiochemical changes during these processes. In particular, surface profile measurement was used for the first time to study these processes. In addition, thermogravimetric analysis was performed to study the kinetics of desorption. Phenomenological models have been formulated to describe the kinetics of intercalation and desorption. The model of intercalation describes interface-controlled intercalation and allows for the first

time a coherent explanation of the various physiochemical changes that accompany intercalation. The model of desorption considers the out-diffusion of the intercalate and gives the first quantitative description of the desorption process. The activation energy for desorption was determined to be 17 kcal/mol below the intralayer order–disorder transformation temperature and 4 kcal/mol above this temperature.

Acknowledgments

Support from the Materials Research Laboratory Section, Division of Materials Research, National Science Foundation, under Grant No. DMR76-81561 A01 is gratefully acknowledged.

References

1 J. G. Hooley, W. P. Garby and J. Valentine, *Carbon, 3* (1965) 7.
2 J. G. Hooley and J. L. Smee, *Carbon, 2* (1964) 135.
3 J. G. Hooley, *Carbon, 10* (1972) 155.
4 G. A. Saunders, A. R. Ubbelohde and D. A. Young, *Proc. R. Soc. London, Ser. A, 271* (1963) 499.
5 G. A. Saunders, A. R. Ubbelohde and D. A. Young, *Proc. R. Soc. London, Ser. A, 271* (1963) 512.
6 G. A. Saunders, *Ph. D. Thesis*, University of London, 1962.
7 R. R. Chianelli, *J. Cryst. Growth, 34* (1976) 239.
8 D. E. Nixon, G. S. Parry and A. R. Ubbelohde, *Proc. R. Soc. London, Ser. A, 291* (1966) 324.
9 T. Sasa, Y. Takahashi and T. Mukaibo, *Carbon, 9* (1971) 407.
10 M. B. Dowell, *Mater. Sci. Eng., 31* (1977) 129.
11 I. L. Spain, A. R. Ubbelohde and D. A. Young, *J. Chem. Soc.*, (1964) 920.
12 G. R. Hennig, in F. A. Cotton, (ed.), *Progr. Inorg. Chem., 1* (1959) 125.
13 J. G. Hooley, *Chem. Phys. Carbon, 5* (1969) 321.
14 W. Metz and D. Hohlwein, *Carbon, 13* (1975) 87.
15 S. H. Anderson, J. S. Culik and D. D. L. Chung, *Ext. Abstr. Program–Bienn. Conf. Carbon, 14* (1979) 262.
16 J. Crank, *Mathematics of Diffusion*, Oxford Univ. Press, London, 1957.
17 S. Aronson, *J. Inorg. Nucl. Chem., 25* (1963) 907.
18 A. B. Kuper, D. Lazarus, J. R. Manning and C. T. Tomizuka, *Phys. Rev., 104* (1956) 1536.